Title

Observation of spin-orbit magnetoresistance in metallic thin films on magnetic insulators

Journal

Science Advances, 4(1)

ISSN

2375-2548

Authors

Zhou, Lifan

Song, Hongkang

Liu, Kai

et al.

Publication Date

2018-01-05

DOI

10.1126/sciadv.aao3318

APPLIED PHYSICS

Observation of spin-orbit magnetoresistance in metallic thin films on magnetic insulators

Lifan Zhou,[1]* Hongkang Song,[2,3]* Kai Liu,[3] Zhongzhi Luan,[1] Peng Wang,[1] Lei Sun,[1] Shengwei Jiang,[1] Hongjun Xiang,[3,4] Yanbin Chen,[1,4] Jun Du,[1,4] Haifeng Ding,[1,4] Ke Xia,[2] Jiang Xiao,[3,4,5†] Di Wu[1,4†]

A magnetoresistance (MR) effect induced by the Rashba spin-orbit interaction was predicted, but not yet observed, in bilayers consisting of normal metal and ferromagnetic insulator. We present an experimental observation of this new type of spin-orbit MR (SOMR) effect in the Cu[Pt]/$Y_3Fe_5O_{12}$ (YIG) bilayer structure, where the Cu/YIG interface is decorated with nanosize Pt islands. This new MR is apparently not caused by the bulk spin-orbit interaction because of the negligible spin-orbit interaction in Cu and the discontinuity of the Pt islands. This SOMR disappears when the Pt islands are absent or located away from the Cu/YIG interface; therefore, we can unambiguously ascribe it to the Rashba spin-orbit interaction at the interface enhanced by the Pt decoration. The numerical Boltzmann simulations are consistent with the experimental SOMR results in the angular dependence of magnetic field and the Cu thickness dependence. Our finding demonstrates the realization of the spin manipulation by interface engineering.

INTRODUCTION

Relativistic spin-orbit interaction (SOI) plays a critical role in a variety of interesting phenomena, including the spin Hall effect (SHE) (*1*–*3*), topological insulators (*4*), and the formation of skyrmions (*5*, *6*). In SHE, a pure spin current transverse to an electric current can be generated in conductors with strong SOI, such as Pt and Ta (*7*, *8*). The inverse SHE (ISHE) is generally used to detect the spin current electrically by converting a pure spin current into a charge current (*9*, *10*). It was recently discovered that the interplay of the SHE and ISHE in a nonmagnetic heavy metal (NM) with strong SOI in contact with a ferromagnetic insulator (FI) leads to an unconventional magnetoresistance (MR)—the spin Hall magnetoresistance (SMR), in which the resistance of the NM layer depends on the direction of the FI magnetization M (*11*–*13*). SMR has been observed in several NM/FI systems and even in metallic bilayers (*14*–*17*). However, it has been argued that SMR may originate from the magnetic moment in the NM layer induced by the magnetic proximity effect (MPE) (*18*). These two mechanisms were proposed to be distinguished by the angular-dependent MR measurements (*11*, *13*). Very recently, another type of MR, the Hanle MR (HMR), was demonstrated in a single metallic film with strong SOI owing to the combined actions of SHE and Hanle effect (*19*). HMR depends on the direction and the strength of the external magnetic field H, rather than that of M in SMR. Within the framework of SMR, because of the negligible SOI in Cu (*20*), one would not expect any MR effect in a Cu/FI bilayer.

Recently, Grigoryan *et al.* (*21*) predicted a new type of MR effect in the NM/FI systems when a Rashba-type SOI is present at the interface between NM and FI. This new spin-orbit MR (SOMR) works even with light metals such as Cu or Al, with negligible bulk SOI, provided that the Rashba SOI is present at the NM/FI interface. However, because of the identical angular dependence on M direction for SOMR and SMR, it is difficult to distinguish SOMR from SMR in systems like Pt/$Y_3Fe_5O_{12}$ (YIG), where both SOMR and SMR are present in principle. Here, we report the first observation of SOMR in a Cu/YIG bilayer, where the Rashba SOI at the Cu/YIG interface is enhanced by an ultrathin Pt layer (<1 nm). We also confirmed that SOMR almost disappears when Pt is placed inside or on the other side of the Cu layer, indicating that SMR from the ultrathin Pt layer cannot be the origin of the observed MR and that the Pt decoration of the Cu/YIG interface is crucial for SOMR. The observed SOMR has the same angular dependence as the SMR in Pt/YIG, in agreement with the SOMR prediction (*21*). The monotonous Cu thickness dependence of SOMR is different from the nonmonotonous dependence of SMR (*13*, *18*). Both the angular and Cu thickness dependences of the observed MR are in good agreement with our Boltzmann simulations based on the SOMR mechanism. In addition, the MR shows two maxima as the Pt layer thickness increases, in sharp contrast to that of SMR (*13*, *22*).

RESULTS AND DISCUSSION

Sample morphology and structure

The YIG films used in this study are 10 nm thick, unless otherwise stated, and grown by pulsed laser deposition (PLD) on $Gd_3Ga_5O_{12}$ (GGG) (111) substrates. The surface morphology of the YIG films was characterized by atomic force microscopy (AFM), as shown in Fig. 1A. The film is fairly smooth with a root mean square (RMS) roughness of 0.127 nm and a peak-to-valley fluctuation of 0.776 nm. The 0.4-nm-thick Pt layer, thinner than the peak-to-valley value of the YIG film, deposited on YIG by magnetron sputtering forms the nanosize islands with an RMS roughness of ~0.733 nm, as shown in Fig. 1B. This discontinuous Pt layer is nonconductive with a resistance over the upper limit of a multimeter. The surface roughness is reduced after the deposition of Cu onto Pt, as shown in fig. S1. Figure 1C presents the cross-sectional high-resolution transmission electron microscopy (HRTEM) image of the Au(3)/Cu(4)[Pt(0.4)]/YIG films, where the numbers are the thicknesses in nanometers. The YIG film is single-crystalline and smooth. The lattice constant of the YIG film is determined to be

[1]National Laboratory of Solid State Microstructures and Department of Physics, Nanjing University, Nanjing 210093, P. R. China. [2]Department of Physics, Beijing Normal University, Beijing 100875, P. R. China. [3]Department of Physics and State Key Laboratory of Surface Physics, Fudan University, Shanghai 200433, P. R. China. [4]Collaborative Innovation Center of Advanced Microstructures, Nanjing 210093, P. R. China. [5]Institute for Nanoelectronics Devices and Quantum Computing, Fudan University, Shanghai 200433, P. R. China.
*These authors contributed equally to this work.
†Corresponding author. Email: xiaojiang@fudan.edu.cn (J.X.); dwu@nju.edu.cn (D.W.)

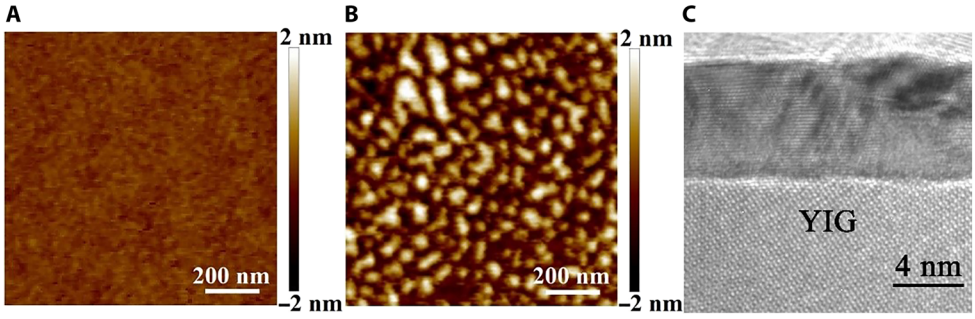

Fig. 1. Sample characterization. (**A**) AFM image of YIG(10)/GGG (RMS roughness, 0.127 nm). (**B**) AFM image of Pt(0.4)/YIG(10)/GGG (RMS roughness, 0.733 nm). (**C**) HRTEM image of the Au(3)/Cu(4)[Pt(0.4)]/YIG heterostructure, where Au is used to prevent the oxidation.

1.2234 nm, as compared to 1.2366 nm for the bulk YIG. A clear interface is observed between the metallic films and the YIG film. The metallic films are polycrystalline.

Field-dependent magnetization and transport measurements

Here, all the measurements were performed at room temperature. The YIG film is almost isotropic in the film plane, with a coercivity of about 0.4 Oe, as shown in Fig. 2A. Because of the large paramagnetic background of the GGG substrate, the magnetization of a thin YIG/GGG film in the out-of-plane geometry is difficult to measure. We measured the 400-nm-thick YIG/GGG(111) film instead. As shown in Fig. 2B, the magnetization is saturated at ~1800 Oe. The saturation magnetization M_s of our YIG film is determined to be 164.5 emu/cm^3, as measured by ferromagnetic resonance (FMR) (see the Supplementary Materials). In comparison, M_s of bulk YIG is 140 emu/cm^3.

Figure 2 (C and D) presents the resistivity ρ as a function of H for the Cu(2)[Pt(0.4)]/YIG(10) sample. In experiments, H was applied (i) along the direction of the current I (x axis), (ii) in the sample plane and perpendicular to the current direction (y axis), and (iii) perpendicular to the sample plane (z axis). The MR effects are present in all measurements. For H along x and y directions, ρ shows two peaks around the coercive fields of YIG. For H along z direction, ρ shows a minimum at $H = 0$ and remains almost a constant value above the saturation field. These features indicate that the MR effects are intimately correlated with M, meaning that the observed MR effects are not HMR.

Angular-dependent MR measurements

To further study the anisotropy of the MR effects in Cu[Pt]/YIG, we performed the angular-dependent MR measurements. Figure 3A shows Δρ/ρ of the Cu(3)[Pt(0.4)]/YIG(10) sample with rotation of H in the xy (α scan), yz (β scan), and xz (γ scan) planes, where α, β, and γ are the angles between H and x, z, and z directions, respectively, as defined in the inset of Fig. 3A. The applied magnetic field strength ($H = 1.5$ T) is large enough to align M with H. The MR effect is anisotropic. The MR ratio, defined as $\Delta\rho/\rho = [\rho(\text{angle}) - \rho(\text{angle} = 90°)]/\rho(\text{angle} = 90°)$, in α and β scans is about 0.012%, which is comparable to the SMR ratio in Pt/YIG (see fig. S3) (*11*, *13*, *23*).

Next, we investigated the origin of the observed MR effect. Considering that Pt on YIG may suffer from the MPE-induced ferromagnetic moment and the corresponding anisotropic MR (AMR) (*24*), we replaced Pt by a 0.4-nm-thick Au layer, which is well known to have a negligible MPE (*25*). The MR effect of 0.002% still appears as shown in Fig. 3B, comparable to the SMR ratio in Au/YIG (see fig. S4), ruling out MPE as the origin of the observed MR. Furthermore, the MR ratios of

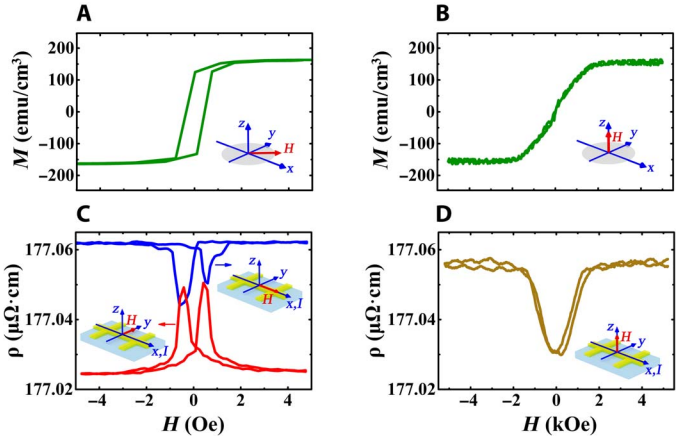

Fig. 2. Field-dependent magnetization and transport measurements. Magnetic hysteresis loops of (**A**) YIG(10)/GGG with field in-plane and (**B**) YIG (400)/GGG with field out-of-plane. ρ measured on the Cu(2)[Pt(0.4)]/YIG(10)/GGG sample for H applied along the (**C**) x axis, y axis, and (**D**) z axis, respectively.

the Cu(3)[Pt(0.4)]/YIG(10) sample in α and β scans are comparable and almost one order of magnitude larger than the MR ratio in the γ scan. This is different from AMR of a ferromagnetic metal, where the MR ratio in α and γ scans is much larger than that in the β scan (*11*, *14*, *24*). Therefore, the MPE-induced AMR can be ruled out.

The behaviors of the MR angular dependence follow the SMR scenario well (*11*, *13*–*15*, *17*). However, with several control experiments, we can unambiguously exclude SMR as the explanation for our observations.

First, the observed MR amplitude cannot be explained by SMR. In our samples, the 0.4-nm-thick ultrathin Pt layer is nonconductive, and the conductivity of bulk Pt is about one order of magnitude smaller than that of bulk Cu, meaning that the current mainly passes through the Cu layer. We prepared a 3-nm-thick single-layer Cu on YIG without interface decoration and performed the MR angular-dependent measurement in the α scan. MR is not observed, as shown in Fig. 3B, evidencing that the Pt-decorated interface is indispensable. A conductive 0.4-nm-thick Pt layer is not available experimentally. Considering that a small fraction of current may flow in the Pt islands, there is a possibility of the occurrence of SMR from the Pt islands. According to the reported SMR results in Pt/YIG bilayers, the SMR ratio in Pt/YIG decreases rapidly with decreasing Pt thickness when the Pt thickness is less than about 3 nm (*13*, *18*). The SMR ratio of Pt(0.4)/YIG is extrapolated to be well below 0.01% from the previously reported Δρ/ρ versus Pt thickness data (*13*, *18*). Considering the pronounced shunting current of the highly

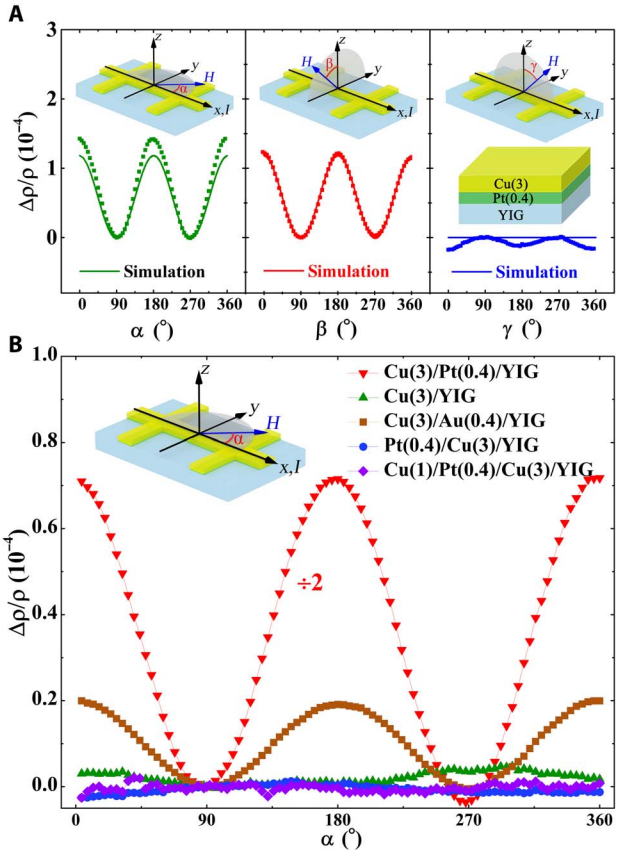

Fig. 3. Angular-dependent MR measurements. (**A**) Angular-dependent MR measurements in the *xy*, *yz*, and *xz* planes for Cu(3)[Pt(0.4)]/YIG. The solid lines are the Boltzmann simulation results. (**B**) Angular-dependent MR measurements in the *xy* plane for several control samples.

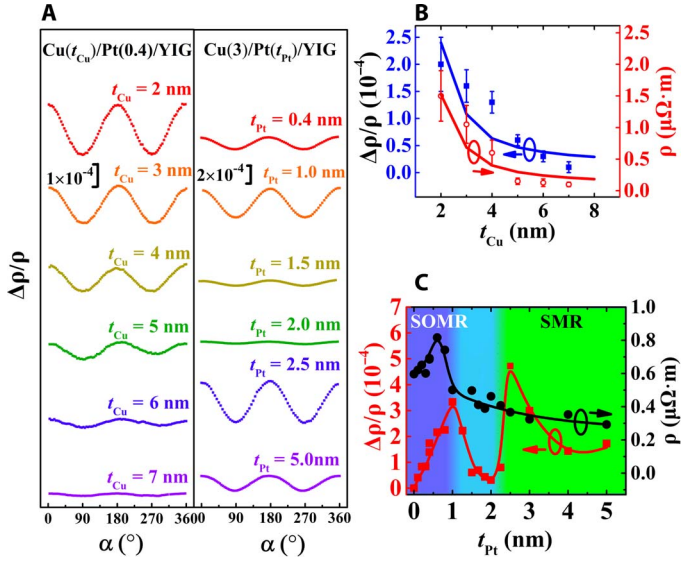

Fig. 4. Cu thickness– and Pt thickness–dependent transport measurements. (**A**) Angular-dependent MR measurements in the *xy* plane for Cu(t_{Cu})[Pt(0.4)]/YIG and Cu(3)/Pt(t_{Pt})/YIG samples. (**B**) Cu thickness dependence of the MR ratio and ρ for Cu(t_{Cu})[Pt(0.4)]/YIG. The solid lines are the Boltzmann simulation results. (**C**) Pt layer thickness dependence of the MR ratio and ρ for Cu(3)/Pt(t_{Pt})/YIG. The solid lines are guide to the eyes.

conductive Cu layer, the SMR ratio should be significantly reduced in Cu[Pt]/YIG, that is, much less than 0.01%. In comparison, the MR ratio is as large as ~0.012% in Cu(3)[Pt(0.4)]/YIG (see Fig. 3A). Therefore, the SMR mechanism cannot explain our observations.

Second, the potential enhancement of SMR caused by intermixing or alloying between a strong SOI material and a weak SOI material can be excluded (*17*, *26*, *27*). For this purpose, we prepared two types of control samples, with the 0.4-nm-thick Pt layer either on top of or inserted inside the Cu layer: [Pt(0.4)]Cu(3)/YIG and Cu(1)[Pt(0.4)]Cu(3)/YIG. Because both samples are fabricated under the same condition as the Cu[Pt]/YIG samples, the intermixing of Pt and Cu should be similar. The MR vanishes in the [Pt(0.4)]Cu(3)/YIG and Cu(1)[Pt(0.4)]Cu(3)/YIG samples, as shown in Fig. 3B. These results rule out the Pt-Cu alloying–induced SMR. Thus, we conclude that the observed MR effect is not SMR.

Cu thickness–dependent transport measurements

To identify the physical origin of the observed unusual MR, we carried out the Cu thickness–dependent measurements. Figure 4A presents the angular-dependent MR measurements of Cu(t_{Cu})[Pt(0.4)]/YIG in α scans for various Cu thicknesses (t_{Cu}). Obviously, the MR ratio steadily decreases with increasing t_{Cu}, highlighting the importance of the Pt-decorated Cu/YIG interface. The monotonous NM thickness dependence of this MR is in sharp contrast to the nonmonotonous behavior of SMR, which peaks at ~3 nm for Pt/YIG (*13*, *18*). The Cu thickness dependence of ρ and the MR ratio extracted from Fig. 4A are shown in Fig. 4B. For very thin Cu film ($t_{Cu} \leq 5$ nm), ρ dramatically increases with decreasing t_{Cu}, indicating that ρ is dominated by the interface/surface scatterings.

Besides SMR, there is another type of MR recently predicted, which has the same angular dependence as we found (see Fig. 3A) (*21*). It originates from the Rashba SOI at the interface of an NM/FI bilayer. By comparing the samples of Cu[Pt]/YIG, [Pt]Cu/YIG, and Cu[Pt]Cu/YIG, one can see that only the Cu[Pt]/YIG samples exhibit a significant MR (see Fig. 3B). It strongly suggests that the MR observed in our experiments is the SOMR predicted by Grigoryan *et al.* (*21*) and that the Pt decoration enhances the Rashba SOI at the Cu/YIG interface.

First-principles calculations and Boltzmann simulations

To prove that the Pt decoration can induce Rashba SOI at the Cu/YIG interface, we carried out first-principles band structure calculations based on (i) a Cu ultrathin film of 14 monolayers, (ii) the same Cu film as (i) but covered by Au on surfaces on both sides, (iii) the same Cu film as (i) but covered by Pt on both surfaces, and (iv) the Pt layer inside the Cu film. By comparing these four different scenarios, we can see that there is no clear Rashba effect in the bare Cu film and the one covered by Au. A strong Rashba effect appears only for Pt on the Cu film surface (the details of calculations are given in the Supplementary Materials).

For a quantitative analysis, we use a Boltzmann formalism to calculate the charge and spin transport in an NM/FI bilayer structure. We solve the following spin-dependent Boltzmann equation in the NM layer

$$\mathbf{v}_0(\mathbf{k}) \cdot \frac{\partial f_\alpha(\mathbf{r},\mathbf{k})}{\partial \mathbf{r}} - e\mathbf{E}\cdot\mathbf{v}_0(\mathbf{k})\,\delta_{\alpha,0} = -R_\alpha(\mathbf{k}) f_\alpha(\mathbf{r},\mathbf{k}) + \sum_{\alpha'=0,x,y,z} \int_{FS} d\mathbf{k}' P_{\alpha,\alpha'}(\mathbf{k},\mathbf{k}') f_{\alpha'}(\mathbf{r},\mathbf{k}') \quad (1)$$

where $f_{\alpha=0,x,y,z}(\mathbf{r},\mathbf{k})$ is the four-component distribution function denoting the charge/spin occupation at position **r** and wave vector **k.** The interface at FI $z = z_+$ contains a Rashba-type SOI described by the Hamiltonian: $H_R = \eta\hat{\sigma}\cdot(\hat{\mathbf{z}} \times \hat{\mathbf{p}})\delta(z - z_+)$, where η is the strength of the Rashba SOI, $\hat{\mathbf{z}}$ is the normal direction of the interface, and $\hat{\mathbf{p}}$ is the momentum operator. H_R gives rise to an anomalous velocity localized at the interface. The Boltzmann equation is solved by discretizing the spherical Fermi surface of Cu and the real space in the *z* direction of Cu film. Using the full distribution function, we calculate all charge/spin transport properties, including the longitudinal and transverse conductivities. This method extends the earlier Boltzmann method developed for current perpendicular-to-plane structure–like spin valves to current in-plane structure–like NM/FI bilayers (*28*–*31*) by taking into account the surface roughness and Rashba SOI at the interface. The details of the simulations are given in the Supplementary Materials.

In the numerical Boltzmann calculation, there are only two fitting parameters: the surface roughness and the Rashba coupling constant. All other parameters either are given by the experiment (such as the film thickness) or can be determined otherwise (such as the bulk relaxation time). Using the quantum description of the rough surface (*32*–*34*), we are able to fit the thickness dependence of ρ in the ultrathin Cu film to a reasonably good precision, as shown in Fig. 4B. It is quite surprising considering that there is only one fitting parameter—the surface roughness. Once the surface roughness is determined, we can calculate the magnetization angular dependence of ρ, in good agreement with the experimental results (see Fig. 3A), from which we obtain the SOMR ratio. The calculated SOMR ratio is shown in Fig. 4B, which demonstrates monotonic decreasing behavior as a function of Cu film thickness, consistent with our experimental results but very different from the non-monotonic behavior observed in SMR (*13*, *18*).

Pt thickness–dependent MR measurements

Finally, to further differentiate SOMR from SMR, we carried out the Pt thickness (t_{Pt})–dependent measurements. To reduce the sample fluctuation, we fabricated the YIG films successively under the same condition. Figure 4A shows the angular-dependent MR measurements of Cu(3)/Pt(t_{Pt})/YIG in α scans, with H = 2000 Oe. The MR ratio extracted from Fig. 4A exhibits nonmonotonous behavior with increasing t_{Pt}, as shown in Fig. 4C. Two separate regimes can be identified: (i) the SOMR regime for t_{Pt} < 1 nm and (ii) the conventional SMR regime for t_{Pt} > 2.2 nm (see Fig. 4C). For t_{Pt} < ~0.6 nm, ρ and Δρ/ρ increase with increasing t_{Pt} because the Pt islands not only introduce the interface scattering but also enhance the Rashba SOI. For ~0.6 nm < t_{Pt} < ~1 nm, the Pt islands start to form a complete layer, leading to the reduction of the interface roughness and the rapid decrease of ρ as seen in Fig. 4C. The MR ratio continues to increase in this region because of the enhanced Rashba SOI with increasing Pt coverage on YIG. For ~1 nm < t_{Pt} < ~2 nm, ρ is smaller than the resistivity of Cu/YIG, suggesting that the interface scattering has minor contribution to ρ. Because SOMR is caused by the interface scattering, the MR ratio rapidly drops in this region. A sizable SMR ratio only appears when t_{Pt} > 2 nm in Pt/YIG (*13*, *18*, *22*). Therefore, around t_{Pt} ~ 2 nm, both SOMR and SMR are small, resulting in a minimum in MR. In the SMR regime, the SMR ratio exhibits a maximum, as expected for SMR (*13*, *18*, *22*). This result demonstrates the differences between SOMR and SMR.

A theoretical calculation shows that a rough interface can enhance SHE (*34*). To understand the role of the roughness to the SOMR, we fabricated the control sample of Cu(3)[Ag(0.7)]/YIG. The RMS roughness of Ag(0.7)/YIG is 0.797 nm, as shown in fig. S9A, similar to that of Pt(0.4 nm)/YIG. Owing to the weak SOI in Ag, the Rashba SOI in Cu [Ag]/YIG is expected to be weak. We do not observe any MR effect down to 5×10^{-6} in Cu(3)[Ag(0.7)]/YIG, as shown in fig. S9B. This result means that the rough surface alone cannot cause the SOMR.

CONCLUSIONS

In conclusion, we report the first observation of the SOMR effect predicted recently (*21*) at room temperature in Cu/YIG films with the Pt decoration at the interface. We show that this MR effect is caused by the enhanced Rashba SOI at the Pt-decorated interface. The angular dependence of SOMR is similar to that of SMR, but all other features are different, such as the increasing MR with decreasing Cu thickness. The amplitude of the SOMR ratio is comparable to that of the SMR ratio in Pt/YIG, highlighting the importance of the NM/FI interfaces. Our finding demonstrates the possibility of realizing spin manipulation by interface decoration.

MATERIALS AND METHODS

The single-crystalline YIG films were epitaxially grown on GGG (111) substrates by the PLD technique using a KrF excimer laser with a wavelength of 248 nm. The PLD system was operated at a laser repetition rate of 4 Hz and an energy density of 10 J/cm^2. The distance between the substrate and the target is 50 mm. Before film deposition, the chamber was evacuated to a base pressure of 1×10^{-7} torr. The YIG films were deposited at ~730°C in an oxygen pressure of 0.05 torr. The growth of the YIG films was monitored by in situ reflection high-energy electron diffraction. The structure was further examined by x-ray diffraction and HRTEM. The magnetic properties of all YIG films were characterized using a vibration sample magnetometer. Then, we used magnetron sputtering to deposit polycrystalline metallic films onto the YIG films via dc sputtering at room temperature with a shadow mask to define 0.3-mm-wide and 3-mm-long Hall bars. The deposition rate was calibrated by x-ray reflectivity. After the metallic film deposition, the samples were immediately mounted and transferred into a vacuum chamber for the transport measurements to minimize the metal oxidation. The resistance was measured by a Keithley 2002 multimeter in a four-probe mode. For the angular-dependent MR measurements with a magnetic field of less than 5000 Oe, the resistance was monitored as the magnet was rotated. The angular-dependent MR measurements with a magnetic field larger than 5000 Oe were performed in a physical property measurement system equipped with a rotatory sample holder.

SUPPLEMENTARY MATERIALS

Supplementary material for this article is available at http://advances.sciencemag.org/cgi/content/full/4/1/eaao3318/DC1

section S1. AFM images of Cu(t_{Cu})[Pt (0.4)]/YIG(10)/GGG(111)
section S2. Magnetic properties of the YIG films
section S3. SMR in Pt/YIG
section S4. SMR and AFM image of Au/YIG
section S5. First-principles calculations
section S6. Boltzmann simulations
fig. S1. AFM images of Cu(t_{Cu})[Pt(0.4)]/YIG(10)/GGG (111).
fig. S2. FMR of the YIG films.
fig. S3. SMR in Pt/YIG.
fig. S4. SMR and AFM image of Au/YIG.
fig. S5. The band structures of Cu, Au/Cu/Au, and Pt/Cu/Pt.
fig. S6. The spin textures of outer and inner bands.
fig. S7. The Rashba splitting in Cu/Pt/Cu.
fig. S8. Specular and diffusive interface scattering in the NM/FI bilayer.

fig. S9. AFM image of Ag(0.7)/YIG and MR of Cu(3)[Ag(0.7)]/YIG.
References (*35*–*51*)

REFERENCES AND NOTES

1. J. E. Hirsch, Spin Hall effect. *Phys. Rev. Lett.* **83**, 1834–1837 (1999).
2. Y. K. Kato, R. C. Myers, A. C. Gossard, D. D. Awschalom, Observation of the spin Hall effect in semiconductors. *Science* **306**, 1910–1913 (2004).
3. J. Sinova, S. O. Valenzuela, J. Wunderlich, C. H. Back, T. Jungwirth, Spin Hall effects. *Rev. Mod. Phys.* **87**, 1213–1260 (2015).
4. M. Z. Hasan, C. L. Kane, Colloquium: Topological insulators. *Rev. Mod. Phys.* **82**, 3045–3067 (2010).
5. S. Mühlbauer, B. Binz, F. Jonietz, C. Pfleiderer, A. Rosch, A. Neubauer, R. Georgii, P. Böni, Skyrmion lattice in a chiral magnet. *Science* **323**, 915–919 (2009).
6. X. Z. Yu, Y. Onose, N. Kanazawa, J. H. Park, J. H. Han, Y. Matsui, N. Nagaosa, Y. Tokura, Real-space observation of a two-dimensional skyrmion crystal. *Nature* **465**, 901–904 (2010).
7. S. O. Valenzuela, M. Tinkham, Direct electronic measurement of the spin Hall effect. *Nature* **442**, 176–179 (2006).
8. T. Kimura, Y. Otani, T. Sato, S. Takahashi, S. Maekawa, Room-temperature reversible spin Hall effect. *Phys. Rev. Lett.* **98**, 156601 (2007).
9. O. Mosendz, J. E. Pearson, F. Y. Fradin, G. E. W. Bauer, S. D. Bader, A. Hoffmann, Quantifying spin Hall angles from spin pumping: Experiments and theory. *Phys. Rev. Lett.* **104**, 046601 (2010).
10. A. Azevedo, L. H. Vilela-Leão, R. L. Rodríguez-Suárez, A. F. Lacerda Santos, S. M. Rezende, Spin pumping and anisotropic magnetoresistance voltages in magnetic bilayers: Theory and experiment. *Phys. Rev. B* **83**, 144402 (2011).
11. H. Nakayama, M. Althammer, Y.-T. Chen, K. Uchida, Y. Kajiwara, D. Kikuchi, T. Ohtani, S. Geprägs, M. Opel, S. Takahashi, R. Gross, G. E. W. Bauer, S. T. B. Goennenwein, E. Saitoh, Spin Hall magnetoresistance induced by a nonequilibrium proximity effect. *Phys. Rev. Lett.* **110**, 206601 (2013).
12. Y.-T. Chen, S. Takahashi, H. Nakayama, M. Althammer, S. T. B. Goennenwein, E. Saitoh, G. E. W. Bauer, Theory of spin Hall magnetoresistance. *Phys. Rev. B* **87**, 144411 (2013).
13. M. Althammer, S. Meyer, H. Nakayama, M. Schreier, S. Altmannshofer, M. Weiler, H. Huebl, S. Geprägs, M. Opel, R. Gross, D. Meier, C. Klewe, T. Kuschel, J.-M. Schmalhorst, G. Reiss, L. Shen, A. Gupta, Y.-T. Chen, G. E. W. Bauer, E. Saitoh, S. T. B. Goennenwein, Quantitative study of the spin Hall magnetoresistance in ferromagnetic insulator/normal metal hybrids. *Phys. Rev. B* **87**, 224401 (2013).
14. C. Hahn, G. de Loubens, O. Klein, M. Viret, V. V. Naletov, J. B. Youssef, Comparative measurements of inverse spin Hall effects and magnetoresistance in YIG/Pt and YIG/Ta. *Phys. Rev. B* **87**, 174417 (2013).
15. M. Isasa, A. Bedoya-Pinto, S. Vélez, F. Golmar, F. Sánchez, L. E. Hueso, J. Fontcuberta, F. Casanova, Spin Hall magnetoresistance at Pt/$CoFe_2O_4$ interfaces and texture effects. *Appl. Phys. Lett.* **105**, 142402 (2014).
16. J. Kim, P. Sheng, S. Takahashi, S. Mitani, M. Hayashi, Spin Hall magnetoresistance in metallic bilayers. *Phys. Rev. Lett.* **116**, 097201 (2016).
17. L. K. Zou, S. H. Wang, Y. Zhang, J. R. Sun, J. W. Cai, S. S. Kang, Large extrinsic spin Hall effect in Au-Cu alloys by extensive atomic disorder scattering. *Phys. Rev. B* **93**, 014422 (2016).
18. S. Y. Huang, X. Fan, D. Qu, Y. P. Chen, W. G. Wang, J. Wu, T. Y. Chen, J. Q. Xiao, C. L. Chien, Transport magnetic proximity effects in platinum. *Phys. Rev. Lett.* **109**, 107204 (2012).
19. S. Vélez, V. N. Golovach, A. Bedoya-Pinto, M. Isasa, E. Sagasta, M. Abadia, C. Rogero, L. E. Hueso, F. S. Bergeret, F. Casanova, Hanle magnetoresistance in thin metal films with strong spin-orbit coupling. *Phys. Rev. Lett.* **116**, 016603 (2016).
20. T. M. Dunn, Spin-orbit coupling in the first and second transition series. *Trans. Faraday Soc.* **57**, 1441–1444 (1961).
21. V. L. Grigoryan, W. Guo, G. E. W. Bauer, J. Xiao, Intrinsic magnetoresistance in metal films on ferromagnetic insulators. *Phys. Rev. B* **90**, 161412(R) (2014).
22. S. Meyer, M. Althammer, S. Geprägs, M. Opel, R. Gross, S. T. B. Goennenwein, Temperature dependent spin transport properties of platinum inferred from spin Hall magnetoresistance measurements. *Appl. Phys. Lett.* **104**, 242411 (2014).
23. S. R. Marmion, M. Ali, M. McLaren, D. A. Williams, B. J. Hickey, Temperature dependence of spin Hall magnetoresistance in thin YIG/Pt films. *Phys. Rev. B* **89**, 220404(R) (2014).
24. T. McGuire, R. Potter, Anisotropic magnetoresistance in ferromagnetic 3d alloys. *IEEE Trans. Magn.* **10**, 1109–1138 (1975).
25. D. Qu, S. Y. Huang, J. Hu, R. Wu, C. L. Chien, Intrinsic spin Seebeck effect in Au/YIG. *Phys. Rev. Lett.* **110**, 067206 (2013).
26. M.-H. Nguyen, M. Zhao, D. C. Ralph, R. A. Buhrman, Enhanced spin Hall torque efficiency in $Pt_{100-x}Al_x$ and Pt_{100-x} Hf_x alloys arising from the intrinsic spin Hall effect. *Appl. Phys. Lett.* **108**, 242407 (2016).
27. Y. Niimi, Y. Kawanishi, D. H. Wei, C. Deranlot, H. X. Yang, M. Chshiev, T. Valet, A. Fert, Y. Otani, Giant spin Hall effect induced by skew scattering from bismuth impurities inside thin film CuBi alloys. *Phys. Rev. Lett.* **109**, 156602 (2012).
28. D. R. Penn, M. D. Stiles, Solution of the Boltzmann equation without the relaxation-time approximation. *Phys. Rev. B* **59**, 13338–13346 (1999).
29. M. D. Stiles, A. Zangwill, Noncollinear spin transfer in Co/Cu/Co multilayers. *J. Appl. Phys.* **91**, 6812–6817 (2002).
30. J. Xiao, A. Zangwill, M. D. Stiles, Boltzmann test of Slonczewski's theory of spin-transfer torque. *Phys. Rev. B* **70**, 172405 (2004).
31. J. Xiao, A. Zangwill, M. D. Stiles, A numerical method to solve the Boltzmann equation for a spin valve. *Eur. Phys. J. B* **59**, 415–427 (2007).
32. Z. Tešanović, M. V. Jarić, S. Maekawa, Quantum transport and surface scattering. *Phys. Rev. Lett.* **57**, 2760–2763 (1986).
33. N. Trivedi, N. W. Ashcroft, Quantum size effects in transport properties of metallic films. *Phys. Rev. B* **38**, 12298–12309 (1988).
34. L. Zhou, V. L. Grigoryan, S. Maekawa, X. Wang, J. Xiao, Spin Hall effect by surface roughness. *Phys. Rev. B* **91**, 045407 (2015).
35. P. E. Blöchl, Projector augmented-wave method. *Phys. Rev. B* **50**, 17953–17979 (1994).
36. G. Kresse, J. Furthmüller, Efficiency of ab-initio total energy calculations for metals and semiconductors using a plane-wave basis set. *Comput. Mater. Sci.* **6**, 15–50 (1996).
37. G. Kresse, J. Furthmüller, Efficient iterative schemes for ab initio total-energy calculations using a plane-wave basis set. *Phys. Rev. B* **54**, 11169–11186 (1996).
38. J. P. Perdew, K. Burke, M. Ernzerhof, Generalized gradient approximation made simple. *Phys. Rev. Lett.* **77**, 3865–3868 (1996).
39. P. M. Haney, H.-W. Lee, K.-J. Lee, A. Manchon, M. D. Stiles, Current induced torques and interfacial spin-orbit coupling: Semiclassical modeling. *Phys. Rev. B* **87**, 174411 (2013).
40. R. E. Camley, J. Barnaś, Theory of giant magnetoresistance effects in magnetic layered structures with antiferromagnetic coupling. *Phys. Rev. Lett.* **63**, 664–667 (1989).
41. K. Fuchs, The conductivity of thin metallic films according to the electron theory of metals. *Math. Proc. Cambridge* **34**, 100–108 (1938).
42. E. H. Sondheimer, The mean free path of electrons in metals. *Adv. Physiol. Educ.* **1**, 1–42 (1952).
43. A. F. Mayadas, M. Shatzkes, Electrical-resistivity model for polycrystalline films: The case of arbitrary reflection at external surfaces. *Phys. Rev. B* **1**, 1382–1389 (1970).
44. Y. Namba, Resistivity and temperature coefficient of thin metal films with rough surface. *Jpn. J. Appl. Phys.* **9**, 1326 (1970).
45. E. V. Barnat, D. Nagakura, P.-I. Wang, T.-M. Lu, Real time resistivity measurements during sputter deposition of ultrathin copper films. *J. Appl. Phys.* **91**, 1667–1672 (2002).
46. J.-W. Lim, K. Mimura, M. Isshiki, Thickness dependence of resistivity for Cu films deposited by ion beam deposition. *Appl. Surf. Sci.* **217**, 95–99 (2003).
47. W. Zhang, S. H. Brongersma, O. Richard, B. Brijs, R. Palmans, L. Froyen, K. Maex, Influence of the electron mean free path on the resistivity of thin metal films. *Microelectron. Eng.* **76**, 146–152 (2004).
48. J.-W. Lim, M. Isshiki, Electrical resistivity of Cu films deposited by ion beam deposition: Effects of grain size, impurities, and morphological defect. *J. Appl. Phys.* **99**, 094909 (2006).
49. Y. P. Timalsina, X. Shen, G. Boruchowitz, Z. Fu, G. Qian, M. Yamaguchi, G.-C. Wang, K. M. Lewis, T.-M. Lu, Evidence of enhanced electron-phonon coupling in ultrathin epitaxial copper films. *Appl. Phys. Lett.* **103**, 191602 (2013).
50. Y. P. Timalsina, A. Horning, R. F. Spivey, K. M. Lewis, T.-S. Kuan, G.-C. Wang, T.-M. Lu, Effects of nanoscale surface roughness on the resistivity of ultrathin epitaxial copper films. *Nanotechnology* **26**, 075704 (2015).
51. S. Takahashi, S. Maekawa, Spin current, spin accumulation and spin Hall effect. *Sci. Technol. Adv. Mater.* **9**, 014105 (2008).

Acknowledgments

Funding: L.Z. and D.W. were supported by the National Key R&D Program of China (2017YFA0303202), the National Natural Science Foundation of China (NSFC) (11674159, 51471086, and 11727808), and the National Basic Research Program of China (2013CB922103). H.S. and J.X. acknowledge the support of NSFC (11474065 and 11722430) and the National Key R&D Program of China (2016YFA0300702). K.X. was supported by the National Key R&D Program of China (2017YFA0303300) and NSFC (11734004, 61774017, and 21421003). **Author contributions:** J.X. and D.W. designed and supervised the project. L.Z. and Z.L. prepared the samples. L.Z. performed the transport measurements with support from Z.L., P.W., and S.J. H.S. performed the Boltzmann simulations under the supervision of J.X. and K.X. K.L. performed the first-principles calculations under the supervision of H.X. L.S. and Y.C. were responsible for the HRTEM characterization. J.X., D.W., and L.Z. wrote the manuscript, and J.D., H.X., H.D., and K.X. commented on the manuscript. All authors discussed the results and reviewed the manuscript. **Competing interests:** The authors declare that they have no competing interests. **Data and materials availability:** All data needed to evaluate the conclusions in the paper are present in the paper and/or the Supplementary Materials. Additional data related to this paper may be requested from the authors.

Submitted 12 July 2017
Accepted 29 November 2017
Published 5 January 2018
10.1126/sciadv.aao3318

Citation: L. Zhou, H. Song, K. Liu, Z. Luan, P. Wang, L. Sun, S. Jiang, H. Xiang, Y. Chen, J. Du, H. Ding, K. Xia, J. Xiao, D. Wu, Observation of spin-orbit magnetoresistance in metallic thin films on magnetic insulators. *Sci. Adv.* **4**, eaao3318 (2018).